

Evaluation of Simplified Procedures for Retrieval of Land Surface Reflectance Factors from Satellite Sensor Output

M. Susan Moran and Ray D. Jackson

USDA-ARS, U.S. Water Conservation Laboratory, Phoenix

Philip N. Slater

University of Arizona, Optical Sciences Center, Tucson

Philippe M. Teillet

Canada Centre for Remote Sensing, Ottawa, Ontario

In response to the need for a simple atmospheric correction method and the consequent verification of such a method, an experiment was conducted to acquire a data set suitable for testing atmospheric correction procedures under a variety of atmospheric conditions. Several procedures, including radiative transfer codes (RTCs) with simulated atmospheres, image-based procedures and dark-object subtraction (DOS), were evaluated by comparing surface reflectance factors derived from Landsat Thematic Mapper (TM) digital data with low-altitude, aircraft-based measurements for seven dates over a 1-year period. Acceptable results, approximately ± 0.02 reflectance (1σ RMS), were achieved based on an RTC with appropriate simulated atmospheres. The DOS technique was the least accurate method and, in fact, produced greater error in estimations of near-IR reflectance than no correction at all. Two hybrid approaches,

which combined the image-based nature of DOS with the precision of an RTC, provided sufficient accuracy and simplicity to warrant use for use on an operational basis. Though, these results were probably site-specific (characterized by relatively low aerosol levels and low humidity), they illustrate the feasibility of simple atmospheric correction methods and the usefulness of a diverse data set for validation of such techniques.

INTRODUCTION

Remotely sensed spectral data have long been promoted for earth-monitoring applications, such as land-cover change detection and evaluation of global energy balance. However, in order to fully realize the potential of satellite spectral data for such applications, it is necessary to convert sensor output (termed digital count, DC) to values independent of atmospheric conditions, that is, values of surface reflectance. Currently, such conversions can be accomplished by measuring atmospheric optical depth on the day of satellite over-

Address correspondence to M. Susan Moran, USDA-ARS, U.S. Water Conservation Laboratory, 4331 E. Broadway, Phoenix, AZ 85040.

Received 1 March 1992.

pass and using a radiative transfer code (RTC) to compute the relationship between surface reflectance and radiance at the sensor. This procedure has proven to be accurate (Holm et al., 1989; Moran et al., 1990), but is too expensive and time-consuming to be used on an operational basis.

Several simpler atmospheric correction procedures have been proposed for satellite-based digital data in the visible and near-IR spectrum (Otterman and Fraser, 1976; Singh, 1988; Dozier and Frew, 1981; Kneizys et al., 1988). Simplified procedures vary in the quantity and accuracy of atmospheric data required for applications and few can be applied when no atmospheric data are available. In the absence of measured atmospheric data, one can resort to using an RTC with suitable simulated atmospheres, for example, midlatitude summer atmosphere or standard U.S. atmosphere. Recently, Richter (1990) suggested that a rough estimate of surface reflectance could be obtained based on a catalogue of atmospheric correction functions compiled using an RTC for different simulated atmospheres, aerosol types, solar zenith angles, and ground altitudes. This catalogue could enable "fast" processing of satellite images for instances when no atmospheric data are available. He further refined the estimate with an approximate correction for the adjacency effect using an $N \times N$ pixel window and appropriate weighting functions for the difference in reflectance.

Another option is to derive information about atmospheric conditions directly from the image itself, thus circumventing the need for on-site measurements of atmospheric and site conditions. Image-based approaches to atmospheric correction generally use scene-derived information about the atmosphere, in combination with an RTC, to retrieve surface reflectance factors. For example, Ahern et al. (1977) extracted path radiance (or haze) information using a clear lake present in the scene and then, based on this estimate of path radiance, inferred atmospheric transmittance and downwelling irradiance with a radiative transfer code. This method has proven to be operational and has been incorporated into the software of the Canada Centre for Remote Sensing (CCRS) Image Analysis System (Teillet, 1986).

A simplified version of this method, termed the dark-object subtraction method, has been

used for some applications (Vincent, 1972; Chavez, 1988; 1989). The dark-object subtraction (DOS) method allows path radiance information to be extracted using the darkest object in the scene, not necessarily a clear water body, and circumvents the need for a radiative transfer code by ignoring the transmittance and downwelling irradiance terms. Though this greatly simplifies the atmospheric correction procedure, the error associated with the latter assumptions could be large.

Although there are a multitude of proposals for simplified atmospheric correction procedures in addition to those mentioned here, few have been validated with ground data under different atmospheric conditions. In an attempt to verify a simple linear formulation for retrieving surface reflectance factors from Landsat MSS DCs, Richardson (1982) compiled data from seven separate investigations. Based on this data set, he derived an empirical relation between Landsat MSS DCs and surface reflectance factors for conditions that closely approximated optically thin atmospheres. Though his results have limited application, he illustrated 1) the feasibility of simple atmospheric correction methods and 2) the usefulness of a diverse data set for validation of such techniques.

In response to the need for a simple atmospheric correction method and the consequent verification of such a method, an experiment was designed to acquire a data set suitable for testing atmospheric correction procedures under a variety of conditions. Simultaneous spectral data were acquired using satellite-, aircraft-, and ground-based sensors over large, uniform ground targets for an extended time period. Atmospheric optical depth was measured during each satellite overpass for input to radiative transfer codes for retrieval of surface reflectance factors from satellite DCs. These results were assumed to be the most accurate and were compared with results using simpler atmospheric correction methods that were not dependent on on-site measurements of optical depth. The analysis included corrections based on simulated atmospheres, variations on the method proposed by Ahern et al. (1977), and the dark-object subtraction technique. Three radiative transfer codes were used:

1. Herman-Browning (Herman and Browning, 1965),

2. 5S (Tanré et al., 1985), modified to allow terrain elevations above sea level (Teillet and Santer, 1991),
3. Lowtran7 (Kneizys et al., 1988).

Values of satellite-derived surface reflectance were compared with low-altitude aircraft-based measurements in the visible and near-IR spectral bands.

ATMOSPHERIC EFFECTS IN REMOTE SENSING

The interaction of electromagnetic radiation with the earth's atmosphere is complex. In this section, discussion will be limited to simple interactions within the atmospheric windows of the visible and near-IR spectrum, ignoring atmospheric refraction, turbulence, and polarization. Furthermore, the sky is assumed to be a uniform Lambertian scatterer and the surface is assumed to be a flat, uniform, Lambertian reflector. The assumptions of isotropic sky irradiance and Lambertian surface reflectance are used extensively in remote sensing analysis and are adopted here for purposes of discussion.

Equations (1)–(4) are based on the derivations by Chandrasekhar (1950) and simplifications by

Slater (1980, p. 307). A summary of the notation is given in Table 1.

The spectral radiance from a surface ($L_{g\lambda}$) is a function of the irradiance reaching the surface and the spectral reflectance of the surface. Slater (1980) expressed this relationship as

$$L_{g\lambda} = (\rho_{g\lambda} / \pi) [(E_{o\lambda}) \cos \theta_z e^{(-\delta_\lambda \sec \theta_z)} + E_{d\lambda}], \quad (1)$$

where $\rho_{g\lambda}$ is the spectral reflectance of the ground surface, $E_{o\lambda}$ is the solar spectral irradiance at the top of the earth's atmosphere, θ_z is the angle of the direct solar flux to the surface normal, δ_λ is the spectral extinction optical thickness, and $E_{d\lambda}$ is the downwelling spectral irradiance.

A satellite-based sensor detects the radiance transmitted through the atmosphere to the sensor ($L_{s\lambda}$). This term is a function of the spectral radiance at ground level, the transmittance through the atmosphere, and the upwelling atmospheric spectral radiance due to scattering ($L_{u\lambda}$). This can be expressed as

$$L_{s\lambda} = L_{g\lambda} e^{(-\delta_\lambda \sec \theta_v)} + L_{u\lambda}, \quad (2)$$

where θ_v is the angle between the line from the sensor to the surface and the normal to the surface of interest.

Equations (1) and (2) can be combined to form a single equation describing the interaction

Table 1. Summary of Scientific and Technical Notation

$L_{g\lambda}$	= spectral radiance at ground level ($\text{W m}^{-2} \text{sr}^{-1} \mu\text{m}^{-1}$)
$L_{s\lambda}$	= spectral radiance at the satellite sensor ($\text{W m}^{-2} \text{sr}^{-1} \mu\text{m}^{-1}$)
$E_{d\lambda}$	= downwelling spectral irradiance at the surface due to scattered solar flux in the atmosphere ($\text{W m}^{-2} \mu\text{m}^{-1}$)
$L_{d\lambda}$	= downwelling spectral radiance at the surface scattered in one direction, within a specified field of view ($\text{W m}^{-2} \text{sr}^{-1} \mu\text{m}^{-1}$)
$L_{u\lambda}$	= upwelling atmospheric spectral radiance scattered in the direction of and at the sensor entrance pupil and within the sensor's field of view ($\text{W m}^{-2} \text{sr}^{-1} \mu\text{m}^{-1}$)
$\rho_{g\lambda}$	= spectral reflectance of the surface, assuming atmospheric scattering and absorption were accounted for
$\rho_{g\lambda u}$	= "apparent" spectral reflectance of the surface, assuming no atmosphere (subscript <i>u</i> means uncorrected)
$E_{o\lambda}$	= solar spectral irradiance on a surface perpendicular to the sun's rays outside the atmosphere ($\text{W m}^{-2} \mu\text{m}^{-1}$)
$\tau_{z\lambda}$	= atmospheric transmittance along the path from the sun to the ground surface, where $\tau_{z\lambda} \approx \exp(-\delta_\lambda \sec \theta_z)$ for scattering and weak absorption
$\tau_{v\lambda}$	= atmospheric transmittance along the path from the ground surface to the sensor, where $\tau_{v\lambda} \approx \exp(-\delta_\lambda \sec \theta_v)$ for scattering and weak absorption
δ_λ	= spectral extinction optical depth
θ_z	= angle of incidence of the direct solar flux onto the earth's surface
θ_v	= angle between the line from the sensor to the surface and the normal to the surface of interest
λ	= spectral band
DC	= satellite-based digital count

of incoming solar irradiance with the atmosphere and the surface,

$$\rho_{e\lambda} = [\pi(L_{s\lambda} - L_{d\lambda}) / \tau_{v\lambda}] / [(E_{o\lambda}) \cos \theta_z \tau_{z\lambda} + E_{d\lambda}], \quad (3)$$

where $\tau_{z\lambda}$ and $\tau_{v\lambda}$ are atmospheric transmittance along the solar and the sensor viewing paths, approximately equal to $e^{(-\delta\lambda \sec \theta_z)}$ and $e^{(-\delta\lambda \sec \theta_v)}$, respectively, for scattering and weak absorbers at θ_z and θ_v values less than 70° .

When atmospheric effects are ignored, Eq. (3) simplifies to

$$\rho_{e\lambda} = (\pi L_{s\lambda}) / (E_{o\lambda} \cos \theta_z), \quad (4)$$

where $\rho_{e\lambda}$ signifies uncorrected (or apparent) reflectance. It should be emphasized that Eq. (3) and (4) do not explicitly show multiple atmosphere/surface reflections; however, the actual computations of the terms include this coupling effect. Furthermore, the $L_{d\lambda}$ and $E_{d\lambda}$ terms are a function of the ground reflectance and the atmospheric coupling.

For remote sensing applications, several of the components in Eqs. (3) and (4) are known. The values of $L_{s\lambda}$ can be computed from the output of the sensor (DC) using data from the in-flight calibration mechanism aboard the satellite. Values of $E_{o\lambda}$ have been published for the response functions of the filters in the TM sensor (Slater et al., 1986). The geometric parameter θ_z can be computed from date and time of overpass, and θ_v can be acquired from header data on the computer compatible tape (CCT) with the image data. Thus, when solving for $\rho_{e\lambda}$ using Eq. (3), there are four unknowns: $\tau_{v\lambda}$, $\tau_{z\lambda}$, $E_{d\lambda}$, and $L_{d\lambda}$. These terms can be determined using an RTC with measurements and/or estimates of atmospheric and site conditions. For most remote sensing applications, measurements of atmospheric conditions, such as Rayleigh, aerosol, and ozone optical depths, are not available. In this case, most RTCs provide the option of using simulated atmospheres in which these and other inputs are estimated based on reasonable assumptions.

One factor that has not been taken into account in this discussion is the effect of multiple scattering in the vicinity of the pixel that can reduce the contrast between targets of different reflectance. This aspect is often ignored because the calculations required to account for the adjacency effect are quite complex and are always at the expense of computational time. Furthermore,

there is some evidence that the multiple reflection and lower-order adjacency effects can be ignored if one is interested only in computing vegetation indices, such as the near-IR/red reflectance ratio (Singh, 1988). But such effects could be important when using reflectance factors for other applications, such as scene classification and evaluation of surface energy balance or albedo. In the latter cases, there is increasing evidence that the adjacency effect is not insignificant and should be accounted for in the future development of atmospheric correction algorithms (Kaufman and Fraser, 1984; Kaufman, 1985). Though the image-based procedure suggested by Richter (1990) shows promise as a relatively simple correction, it has not yet been validated with ground-based measurements.

EXPERIMENT

A multidisciplinary, multiagency experiment was conducted at the University of Arizona's Maricopa Agricultural Center (MAC) to collect simultaneous ground-, aircraft-, and satellite-based radiometer measurements over uniform surfaces. From April 1985 to June 1986, atmospheric measurements and aircraft-mounted and ground-based radiometer measurements were made on each day of the Landsat-5 overpass, weather and equipment permitting (Moran, 1986). Landsat TM digital data were ordered if the sky was clear at the zenith and around the sun at the time of satellite overpass. Twelve TM scenes were acquired during the period of the experiment.

Site Description

The experimental site, MAC, is a 770 ha farm located about 48 km south of Phoenix (latitude $33^\circ 03'$, longitude $112^\circ 59'$). The maximum daily air temperature ranges from over 42°C in the summer to less than 15°C in winter. The relative humidity is generally low, with the average monthly value ranging from about 10% in May and June to about 50% during the "monsoon" season in August. The average yearly rainfall is about 20 cm.

The farm is divided into a research and a demonstration area. The research farm is a 162 ha area of multiple plots that are used for small-scale

development projects. The demonstration farm is a 608 ha area, with fields up to 0.27 km \times 1.6 km in size, dedicated to demonstrating new farming techniques on a production scale. All the data for this experiment were acquired in large, uniform, laser-leveled fields located on the MAC demonstration farm. The soil textures included clay loam, sandy loam, and sandy clay loam (Post et al., 1988). Alfalfa is grown year-round with about seven to eight harvests per year; cotton is grown during the summer, and wheat during the winter. MAC is surrounded by similar, flat agricultural land and desert [a photographic image of MAC and the Maricopa area has been presented by Jackson (1990)].

Aircraft-Based Data

Aircraft-based spectral reflectance data were collected along a route designed to cover 12 of the largest MAC fields. Flights were scheduled to coincide with satellite overpasses and ground-based data collections. The aircraft was flown at a nominal altitude of 150 m. The airborne sensors included an Exotech¹ radiometer with TM filters, an infrared thermometer (IRT), and a color video camera mounted to provide a view normal to the ground surface. The video data were used to identify the ground location and surface type for each spectral reflectance datum. A portable data logger signaled the device to collect a sample every 2 s and recorded the time of sampling to 0.0001 h.

Measurements of radiance from a calibrated BaSO₄ panel were recorded by ground-based radiometers during each flight and used to calculate the aircraft-based reflectance factors of the various ground surfaces (Jackson et al., 1987). This was accomplished by comparing the voltages from the ground-based and airborne radiometers over a calibrated reflectance panel before and after each flight, calculating a ratio of aircraft-based to ground-based Exotech voltages, and multiplying the ground-based panel readings by this ratio. Knowing the absolute reflectance calibration of

the panel, the reflectance factors of the various ground surfaces measured from the aircraft could be calculated.

In order to validate the use of aircraft-based reflectance data as a ground reference, a simple comparison of ground- to aircraft-based reflectance factors was conducted by Holm et al. (1989) for this data set. An average of six readings collected by the airborne sensor over a fallow field were compared with the average of 64 corresponding ground-based samples. The reflectance factors were computed as described previously and averaged to produce one reflectance factor for the aircraft-based and ground-based measurements per band. The differences between the ground- and low-altitude aircraft-based reflectance factors were 0.004 or less for the four TM bands. An average difference of 0.006 was obtained by Pinter et al. (1990) for a similar comparison with a different data set.

Satellite-Based Data

The Landsat TM sensor acquires image data at 30 m resolution in four wavelength bands in the visible and near-IR spectrum (TM1, 0.45–0.52 μm ; TM2, 0.53–0.61 μm ; TM3, 0.62–0.69 μm ; and TM4, 0.78–0.90 μm). Seven of the 12 TM images acquired in the MAC experiment were selected for this analysis based on image quality and availability of ancillary data (Table 2). All TM scenes were acquired with Level-A processing from EROS Data Center, Sioux Falls, South Dakota. The Level-A processing consists of a "radiometric" correction to normalize detector response within each of the spectral bands but no "geometric" correction. The radiometric correction of the

Table 2. Satellite Overpass Specifications^a

Date	DOY	θ_z	E_{o1}	E_{o2}	E_{o3}	E_{o4}
23 Jul 85	85204	29.84	1895.1	1770.5	1497.3	1010.6
8 Aug 85	85220	30.08	1895.1	1770.5	1497.3	1010.6
27 Oct 85	85300	50.88	1980.8	1850.5	1565.0	1056.3
20 Mar 86	86079	43.76	1970.9	1841.3	1557.2	1051.0
5 Apr 86	86095	38.35	1953.0	1824.5	1543.0	1041.4
21 Apr 86	86111	33.35	1935.5	1808.2	1529.2	1032.1
24 Jun 86	86175	27.56	1891.0	1766.7	1494.1	1008.4

¹ The use of company names and brand names are necessary to report factually on available data; however, the USDA, UA, and CCRS neither guarantee nor warrant the standard of the product, and the use of the same by USDA, UA, or CCRS implies no approval of the product to the exclusion of others that may also be suitable.

^a DOY refers to day of calendar year, θ_z is the solar zenith angle (in degrees) and $E_{o\lambda}$ is the solar spectral irradiance at the top of the earth's atmosphere ($\text{W m}^{-2} \mu\text{m}^{-1}$), where λ is replaced by numbers 1–4 referring to TM spectral Bands 1–4. Time of overpass was approximately 10:33 MST.

Table 3. Spectral Optical Depth Values in the TM Spectral Bands Estimated for Seven Dates in 1985 and 1986 at MAC*

DOY	TM1			TM2			TM3			TM4		
	Aer	Ray	O ₃									
85204	0.127	0.156	0.009	0.099	0.081	0.039	0.079	0.045	0.019	0.054	0.017	0.002
85220	0.173	0.157	0.006	0.139	0.081	0.026	0.114	0.045	0.013	0.083	0.017	0.002
85300	0.124	0.156	0.006	0.096	0.081	0.025	0.076	0.045	0.012	0.053	0.017	0.001
86079	0.084	0.158	0.008	0.064	0.082	0.034	0.049	0.045	0.017	0.033	0.017	0.002
86095	0.085	0.156	0.012	0.069	0.081	0.052	0.056	0.045	0.017	0.041	0.017	0.003
86111	0.058	0.154	0.005	0.049	0.080	0.030	0.041	0.044	0.013	0.031	0.017	0.000
86175	0.175	0.156	0.013	0.136	0.081	0.054	0.108	0.045	0.027	0.074	0.017	0.003

* DOY refers to the day of year. Aer, Ray, and O₃ are aerosol, Rayleigh, and ozone optical depth values.

TM scenes results in substantial enhancement of the DCs and requires some work (Holm, 1987; Holm et al., 1989) to reverse the correction process. The reversal is necessary in order to use the TM absolute calibration factors to convert DC to radiance.

Atmospheric Measurements

On each overpass date, measurements of incident solar illumination were made with a solar radiometer over the time period from sunrise to solar noon (Slater et al., 1987). Total optical depth of the atmosphere was determined from the slopes

of Langley plots, in which the natural logarithm of the voltages from the solar radiometers was plotted against air masses for several wavelengths throughout the spectral range of interest. Total optical depth was partitioned into Rayleigh, aerosol, and ozone optical depths using the procedure described by Biggar et al. (1990) (Table 3).

DATA PROCESSING

A subset of TM digital counts was selected from each of the TM scenes for correlation with the aircraft-based reflectance factors. Two targets,

Table 4. List of Corresponding Aircraft-Based Reflectance Factors and Landsat5 TM Digital Counts for Bare Soil and Vegetated Targets at MAC*

DOY	Aircraft-Based Reflectance				Landsat TM "Raw" Digital Counts			
	TM1	TM2	TM3	TM4	TM1	TM2	TM3	TM4
<i>Soil</i>								
85204	0.0805	0.1205	0.1684	0.2155	96.33	48.58	64.60	63.02
85220	0.0845	0.1256	0.1854	0.2250	96.69	47.35	62.74	60.57
85300	0.0745	0.0941	0.1082	0.2425	78.40	34.05	37.90	50.13
86079	0.0698	0.1072	0.1539	0.1997	77.55	39.12	52.44	51.30
86095	0.0664	0.0992	0.1498	0.2039	80.38	38.99	52.12	51.09
86111	0.0924	0.1398	0.2061	0.2736	95.85	50.83	71.67	69.15
86175	0.1046	0.1491	0.2101	0.2662	110.51	58.25	80.07	76.11
<i>Vegetation</i>								
85204	0.0232	0.0589	0.0269	0.5387	70.80	32.70	24.07	143.20
85220	0.0302	0.0591	0.0365	0.5861	76.01	32.99	26.94	142.81
85300	0.0953	0.1424	0.1947	0.2437	82.78	41.56	55.91	51.85
86079	0.0260	0.0465	0.0302	0.3758	60.54	24.94	20.20	92.87
86095	0.0370	0.0634	0.0533	0.4124	70.34	31.97	29.47	97.16
86111	0.0235	0.0542	0.0239	0.6258	68.04	30.84	23.26	154.42
86175	0.0310	0.0650	0.0336	0.5713	77.14	35.92	28.08	153.64

* "Raw" DCs refer to DCs for which the radiometric correction applied in the A-tape processing has been reversed. These DCs can be converted to at-satellite radiance using the absolute radiometric calibration coefficients listed in Table 5.

Table 5. Thematic Mapper Sensor Calibration Coefficients*

Date	TM1		TM2		TM3		TM4	
	Mult	Add	Mult	Add	Mult	Add	Mult	Add
Before Oct 1985	13.82	2.79	7.12	3.06	9.25	3.12	10.30	2.73
After Oct 1985	13.89	2.71	7.20	2.56	9.40	2.60	10.35	2.36

* Coefficients are in units of digital count per radiance ($\text{DC} \cdot \text{m}^2 \cdot \text{sr} \cdot \mu\text{m} \cdot \text{W}^{-1}$). "Mult" refers to the multiplicative factor and "Add" to the additive factor.

one bare soil and one full-cover vegetation, were selected from each scene. Uniform subsets from within each target were selected by visual examination of a DC printout of the area. The subsets consisted of 12–36 pixels, which were averaged to obtain a mean DC value for the area. A set of two to five aircraft-based pixels, corresponding spatially to the location of the TM pixels, was averaged to produce a single reflectance factor for each averaged DC value. This resulted in 56 points: two targets per seven scenes per four TM bands (Table 4).

The DCs extracted from the Landsat TM images required some preprocessing (Holm et al., 1989) to reverse the radiometric correction routinely applied by the EROS Data Center. The TM "raw" DCs were then converted to top-of-the-atmosphere radiance (L_{λ}) using the absolute radiometric calibration coefficients of the TM (Slater et al., 1986) (Table 5). The uncorrected or "apparent" surface reflectance factors ($\rho_{\rho\lambda}$) were computed from values of L_{λ} using Eq. (4).

Corrected surface reflectance factors ($\rho_{\rho\lambda}$) were computed using three approaches (summarized in Table 6). In the first, on-site optical depth

measurements were used as input to an RTC to compute surface reflectance factors based on satellite DC values. This method provided the most accurate results, to be used as a baseline for comparison with results from the simpler approaches. Second, $\rho_{\rho\lambda}$ values were retrieved based on RTC output with reasonable simulated atmospheres and a Rayleigh atmosphere. This approach could be an attractive alternative for some remote sensing applications in which atmospheric data are not available. Third, several image-based approaches were tested, including the dark-object subtraction method, to determine the viability of these methods and the necessity of incorporating an RTC into the correction process.

RTC Solution with Measured Input

Two radiative transfer codes (Herman–Browning and 5S) were applied using on-site measurements of atmospheric optical depth (Table 3). For the Herman–Browning code, we used a value of $1.54 - 0.01i$ for the complex refractive index of the aerosols (Jennings et al., 1978) and we assumed a Junge size distribution for aerosol particles (Big-

Table 6. Summary of Atmospheric Correction Abbreviations Used in Text and Figure Captions

UNC	= uncorrected estimates using Eq. (4) (apparent reflectance)
<i>Radiative Transfer Codes (RTC) with Measured Input</i>	
HBC	= Herman–Browning code, using on-site measurements of optical depth
5SC	= 5S code, using on-site measurements of optical depth
<i>RTC with Simulated Input</i>	
L-M	= Lowtran7 (L7) code using the midlatitude summer model default
L-S	= L7 code using the standard U.S. atmosphere model default
L-R	= Lowtran7 code using a Rayleigh atmosphere with only gas absorption
<i>Image-Based Correction Methods with and without Use of RTC</i>	
DOS	= dark-object subtraction based on the image histogram (assume dark object $\rho_{\rho\lambda} = 0.01$)
5SD	= 5S code with input based on dark-object information (assume dark object $\rho_{\rho\lambda} = 0.01$)
L-D	= L7 code with simulated atmosphere chosen using dark-object information (assume dark object $\rho_{\rho\lambda} = 0.01$)
5SD2	= same as 5SD, assuming dark object has 0.02 surface reflectance
L-D2	= same as L-D, assuming dark object has 0.02 surface reflectance

gar et al., 1990). The aerosol profile was based on measurements at White Sands, New Mexico (Elterman, 1968), the O_3 and H_2O profiles were based on work by Mateer et al. (1980) and Sissenwine et al. (1968), respectively. The atmospheric pressure profile was based on the Standard 1962 U.S. Atmosphere. Scattering computations were determined at the nominal spectral band center (Palmer, 1984). For the 5S code, the continental aerosol and midlatitude summer atmospheric profiles were assumed, and the aerosol optical depth at 550 nm was derived from the Junge parameter computed for the Herman-Browning code. Satellite-derived surface reflectances ($\rho_{g\lambda}$) were determined by fitting RTC-calculated $L_{s\lambda}$ values to the image-derived $L_{s\lambda}$ values, assuming different values for the surface reflectance in the RTC.

RTC Solution with Simulated Input

The Lowtran7 RTC was applied by selecting suitable, simulated atmospheric models to describe radiative transfer conditions. Three different models were selected:

1. Midlatitude summer model,
2. Standard U.S. atmosphere model,
3. Rayleigh atmosphere with zero water vapor and estimates of gaseous absorption.

A comparison of vertical profiles of air temperature, pressure and relative humidity for each atmospheric model on 23 July is presented in Figure 1. Note that all three models produce similar estimates of atmospheric pressure, corresponding well with the on-site measurement of barometric pressure. None of the models produced ground-level air temperatures as high as those recorded at MAC during July. For the Rayleigh atmosphere, the ground-level air temperature was used as input to the model, and thus the results showed good agreement at ground level. The relative humidity was overestimated by both the standard U.S. model and midlatitude summer models. The Rayleigh model, by definition, assumed that there was no atmospheric water vapor absorption.

Image-Based Solutions, with and without Use of RTC

The path radiance term (L_{dn}) was estimated from TM image data using the lower bounds of histo-

grams generated for each band from a TM quarter-scene, covering a 90 km \times 90 km area on the ground. Histograms were characterized by a gradual increase in the number of pixels starting at some nonzero DC values. The lower-bound of the histogram (or "dark object") was assumed to be indicative of the amount of upwelling path radiance in that band. The surface reflectance of the dark object was assumed to be 0.01 for all scenes and all bands, based on computations using the Herman-Browning code with on-site measurements of optical depth. Thus, the path radiance was assumed to be the dark-object radiance minus the radiance contributed by 0.01 surface reflectance.

These path radiance values were then used to do a dark-object subtraction correction. That is, $\rho_{g\lambda}$ was computed using Eq. (3), where L_{dn} was estimated from the lower bound of the image histogram, the transmittances along the viewing and solar paths were assumed to be 1 ($\tau_{v\lambda} = \tau_{s\lambda} = 1.0$), and the downwelling atmospheric irradiance (E_{dn}) was assumed to be 0.

Two other image-based procedures were explored, a simple method based on Lowtran7 and a more complex procedure based on 5S. Both methods used the histogram lower-bound to estimate L_{dn} , and, as suggested by Ahern et al. (1977), a radiative transfer code was used to infer $\tau_{v\lambda}$, $\tau_{s\lambda}$, and E_{dn} and compute surface reflectance.

For the Lowtran7-based method, the image-based estimates of L_{dn} were used to select the most appropriate atmospheric model from the selections offered by the Lowtran7 code. Then, rather than use Eq. (3) to solve for surface reflectance, $\rho_{g\lambda}$ was computed directly from at-satellite radiance ($L_{s\lambda}$) using the Lowtran7 code with the simulated atmosphere. For example, values of L_{dn} computed using the Lowtran7 code were compared with those estimated using the dark object (Table 7) to select the most suitable Lowtran7 model. Using TM1 as the basis for model selection, according to Table 7, the standard U.S. model would be most appropriate for both 21 April and 24 June.

For the 5S-based method, the 5S code was used iteratively to find the aerosol optical depth corresponding to the path reflectance (including intrinsic atmospheric and surround contributions) obtained from the dark target in each TM spectral band. The resulting aerosol optical depths were subsequently used in 5S runs to retrieve surface

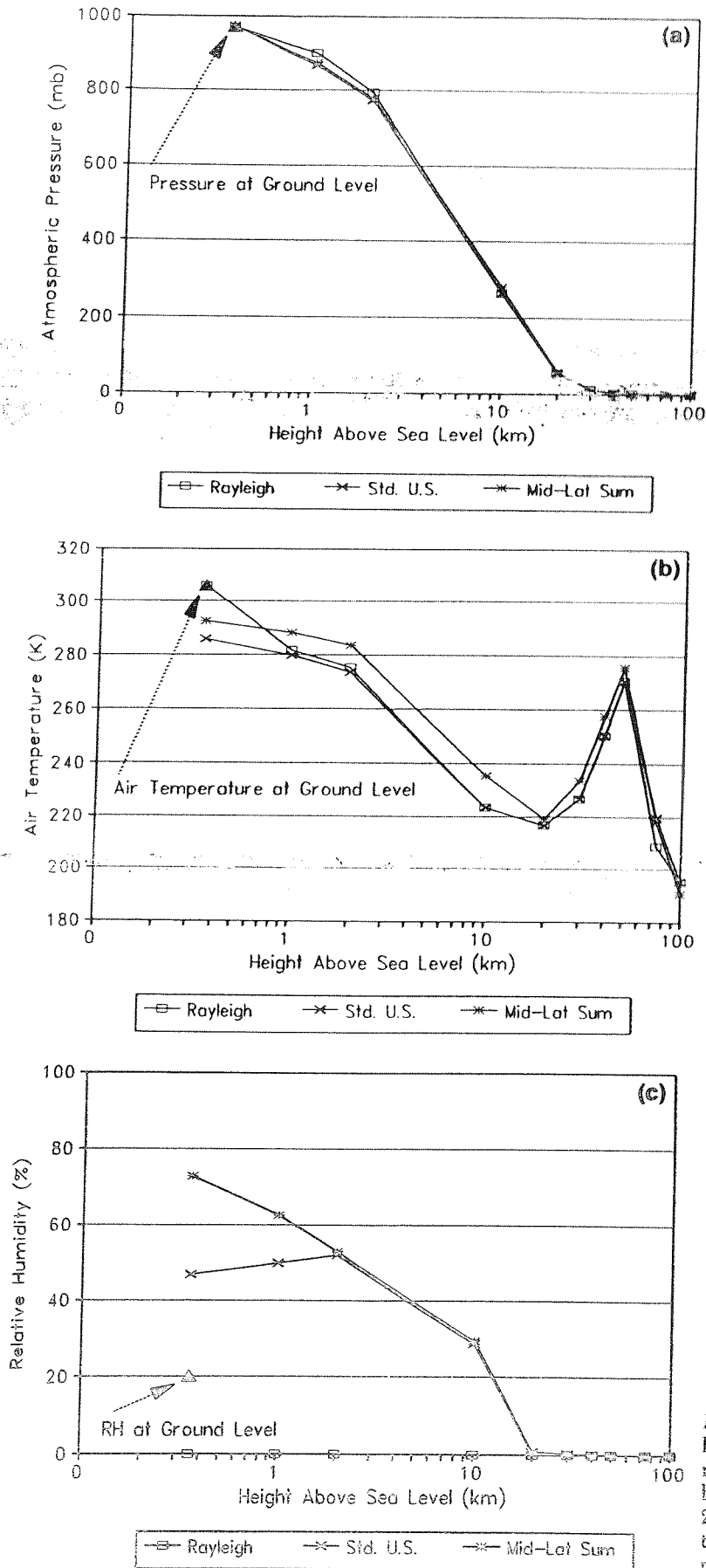


Figure 1. A comparison of the Lowtran7 Rayleigh, midlatitude summer and standard U.S. models for estimation of a) barometric pressure, b) air temperature, and c) relative humidity on 23 July 1985. The arrows (pointing to the solid triangles) designate the on-site measurements of pressure, air temperature, and relative humidity.

Table 7. Values of TMI Upwelling Path Radiance ($W m^{-2} sr^{-1}$) on 21 April 1986 and 24 June 1986, Using the Dark-Object Method and the Lowtran7 Code with Three Simulated Atmospheres

	21 April $L_{d\lambda}$	24 June $L_{d\lambda}$
Lowtran7		
Rayleigh	2.005	2.071
Standard U.S.	2.450	2.519
Midlatitude summer	2.845	2.921
Dark object	2.249	2.701

reflectances for the soil and vegetation cases. In all 5S runs, a continental aerosol and a midlatitude summer atmospheric profile were assumed.

RESULTS AND DISCUSSION

In order to compare the simplified correction procedures with those based on optical depth measurements, the root mean squared (RMS) error and mean difference (Δ_m) of satellite-derived estimates of surface reflectance were computed for each procedure. The RMS error is the standard deviation of the difference between the satellite-based estimates and aircraft-based measurements of surface reflectance. This statistic is helpful in assessing the absolute error associated with each method. The Δ_m is the average of the differences between the satellite-based estimates and aircraft-based measurements of surface reflectance. Though Δ_m underestimates the overall error when positive and negative differences are averaged, it is useful in distinguishing whether the method was over- or undercorrecting the satellite data.

RMS Error of Satellite-Based Reflectance Factor Retrieval

RMS error was computed for each correction method based on reflectance data for the two ground targets, four spectral bands, and seven acquisition dates listed in Table 4. The RMS error of reflectance corrected using the Herman-Browning and 5S radiative transfer codes with on-site measurements of spectral optical depth was nearly 70% less than for uncorrected data (Fig. 2a). The RMS errors of satellite-based reflectance factors were approximately 0.012 reflectance, and the results using either code were not significantly

different. The small error associated with reflectance factor retrieval could be attributed in part to errors in the satellite calibration, the radiative transfer equations, the ground-based measurements of optical depth and the aircraft-based measurements of surface reflectance, and the unknown influence of the adjacency effect.

The Lowtran7 code based on simulated atmospheres produced variable results depending on the suitability of the atmospheric model (Fig. 2b). For example, when the Lowtran7 Rayleigh model (L-R) was applied without accounting for water vapor absorption, the RMS error of $\rho_{p\lambda}$ estimates was greater than 0.02. However, when more complex models were chosen (accounting for water vapor absorption and aerosol scattering), the Lowtran7 code produced results substantially better than the uncorrected values and comparable to the RMS errors presented in Figure 2a. In all cases, the use of radiative transfer codes with simulated atmospheres improved the satellite-derived estimates of reflectance.

The dark-object subtraction method theoretically accounts for the additive effect of atmospheric path radiance. For this data set, the method (DOS in Fig. 2c) resulted in RMS error similar to that for the uncorrected data. A variation on the DOS technique, proposed by Chavez (1988), was also applied to the data but results were not significantly improved. This inaccuracy was due to the DOS assumptions that $\tau_{v\lambda} = \tau_{z\lambda} = 1.0$ and $E_{d\lambda} = 0.0$. The error in surface reflectance estimation associated with the assumption that atmospheric transmittance is 1 [according to Eq. (3)] would be on the order of $1/(\tau_{v\lambda}\tau_{z\lambda})$. Likewise, the assumption that $E_{d\lambda} = 0.0$ can cause considerable error in reflectance estimates. For example, downwelling spectral radiance ($L_{d\lambda}$) can be as large as 25% of $L_{p\lambda}$, even for relatively clear atmospheres (Biggar, 1990). On the other hand, there was relatively good agreement between estimates of $L_{d\lambda}$ based on Lowtran7 code and those determined from the image histogram.

The image-based correction methods based on Lowtran7 and 5S codes (5SD and L-D in Fig. 2c) gave results with RMS errors close to 0.015 reflectance. These results were comparable to those presented in Figures 2a and 2b. These results also reaffirmed the belief that much of the error associated with the DOS technique was due to the assumptions that $\tau_{v\lambda} = \tau_{z\lambda} = 1.0$ and $E_{d\lambda} = 0.0$.

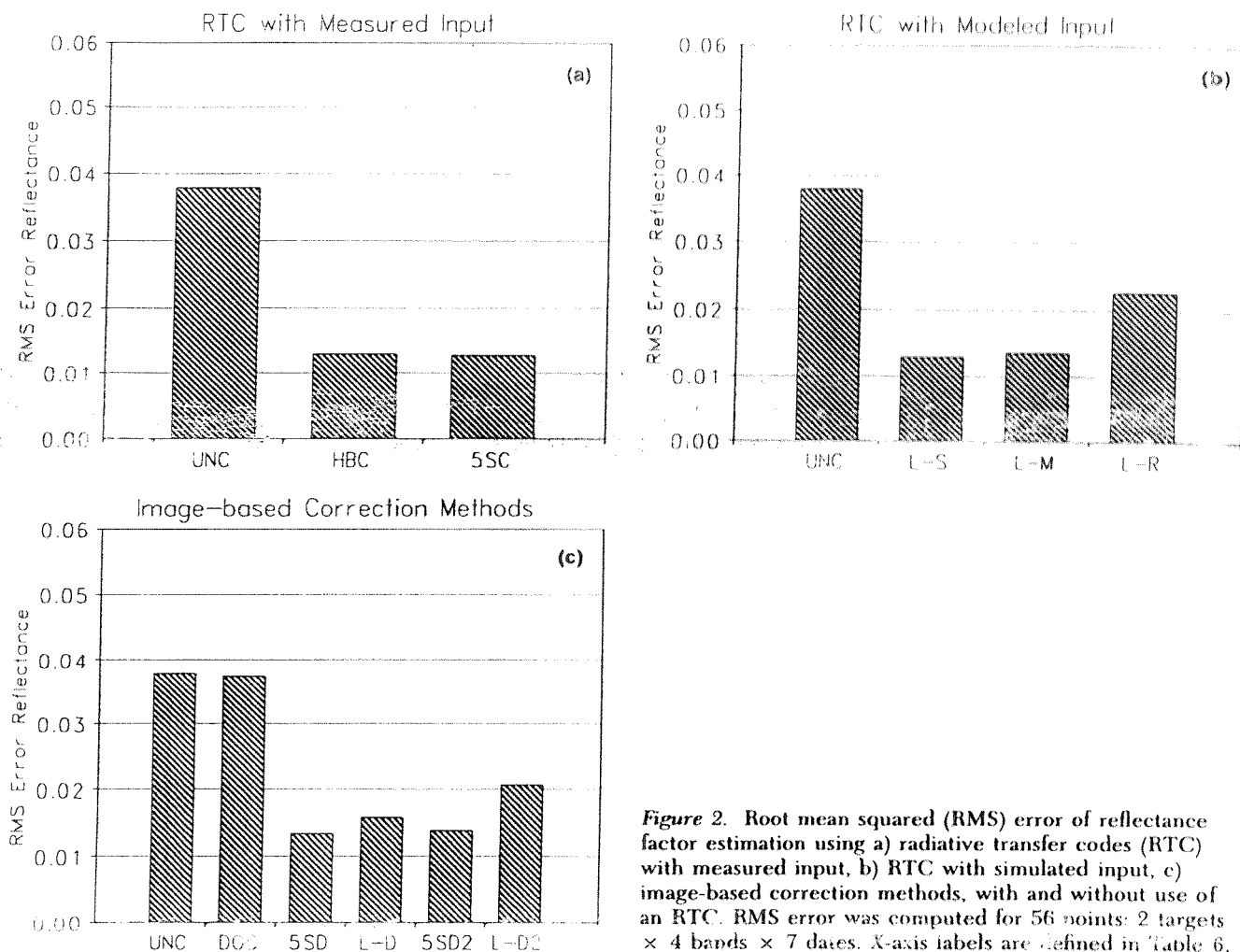


Figure 2. Root mean squared (RMS) error of reflectance factor estimation using a) radiative transfer codes (RTC) with measured input, b) RTC with simulated input, c) image-based correction methods, with and without use of an RTC. RMS error was computed for 56 points: 2 targets \times 4 bands \times 7 dates. X-axis labels are defined in Table 6.

It should be reemphasized at this point that these results are specific to the MAC site, generally characterized by low to moderate aerosol levels and low humidity.

A basic assumption of the DOS, 5SD, and L-D methods was that the surface reflectance of the dark object was 0.01. This assumption was substantiated using the Herman-Browning RTC with on-site measurements of optical depth. In most cases, this sort of verification would not be possible and the image-based techniques would have to be applied with a reasonable "guess" about the dark-object surface reflectance. In order to assess the sensitivity of this parameter on the overall accuracy of the correction procedure, the L-D and 5SD methods were reexamined with the assumption that the dark-object surface reflectance was 0.02 (5SD2 and L-D2 in Fig. 2c). For this data set, the RMS error of L-D2 was

nearly 1.4 times larger than for L-D, increasing to greater than 0.02 RMS error. Changing the dark-object reflectance to 0.02 had very little effect on the RMS error of the 5SD method, probably because the aerosol optical depth was relatively low. However, it did increase the number of nonconvergence cases for which aerosol optical depth was then assumed to be 0.05 at $0.55 \mu\text{m}$. Though image-based corrections, such as 5SD and L-D, are attractive due to their simplicity, it may be necessary to have some knowledge of surface reflectance if accurate results are to be expected.

Error Evaluation by Spectral Band

The mean difference (Δ_m) of satellite- and aircraft-based estimates of surface reflectance was computed for each TM band over all methods

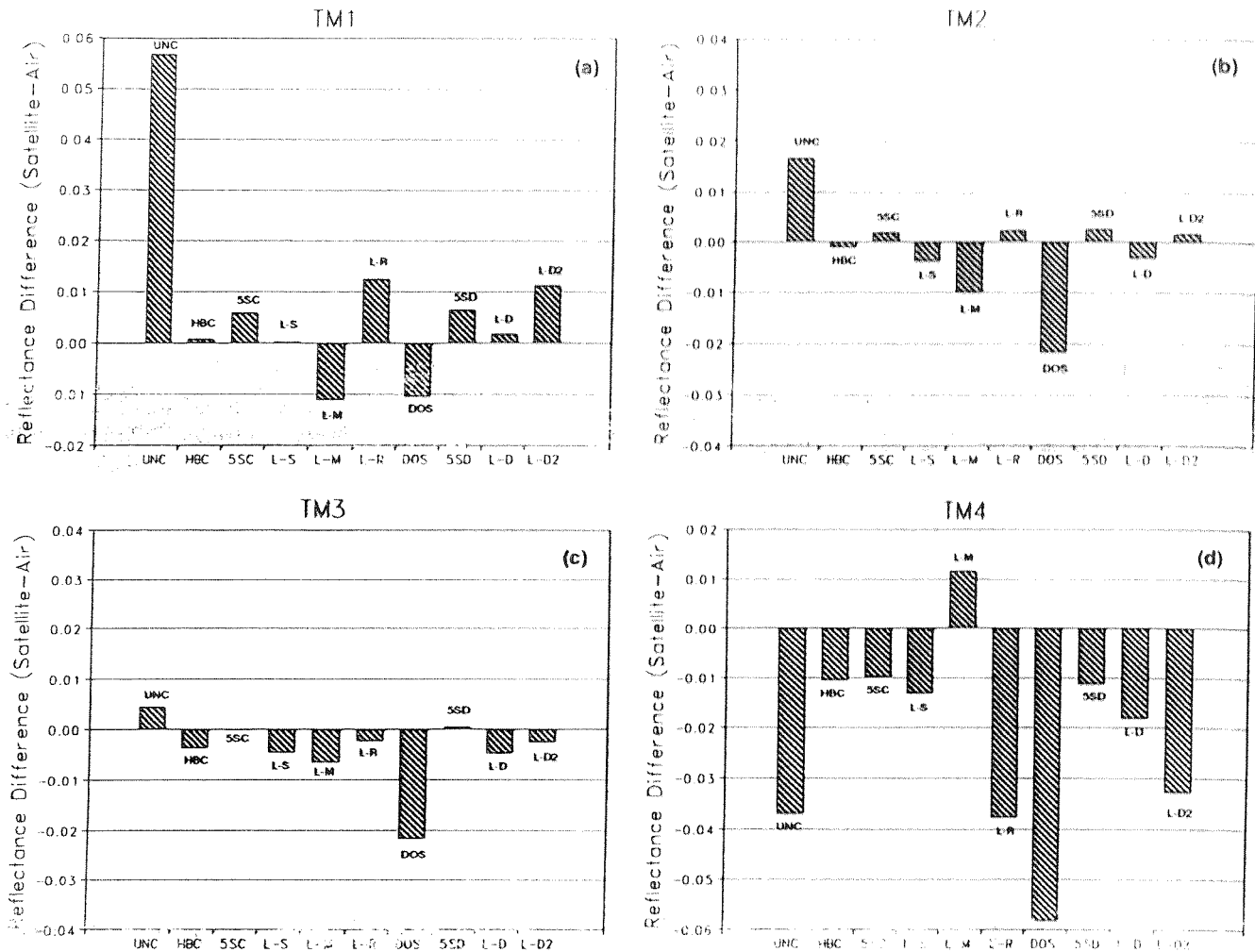


Figure 3. Average reflectance difference (Δ_m) for satellite- and aircraft-based reflectance factors, by spectral band TM1–TM4. Δ_m was computed for 14 points: 2 targets \times 7 dates per band. X-axis labels are defined in Table 6.

(Fig. 3). The relative influence of scattering on shorter wavelengths and absorption on longer wavelengths is apparent in values of Δ_m for uncorrected estimates of surface reflectance (UNC), where reflectance is greatly overestimated in TM1 and underestimated in TM4. The influences of scattering and absorption are offset for the intermediate wavelengths, resulting in low Δ_m values for uncorrected reflectance estimates in TM2 and TM3.

There are several points that can be inferred from data presented in Figure 3. First, all the correction methods worked well for correcting TM1. The Lowtran7 Rayleigh model (L-R) resulted in a slight undercorrection (perhaps due to disregard for aerosol scattering) and the Lowtran7 midlatitude summer model (L-M) overcorrected

the data. Second, all the corrections except DOS worked well for TM2 and TM3. The Δ_m was close to 0.0, indicating very slight over- and undercorrections of the original data. Third, nearly all the methods tended to undercorrect TM4, except the Lowtran midlatitude summer model. Whether over- or undercorrected, the Δ_m was slight for all models, except the L-R and DOS. Neither L-R nor DOS account for water vapor and ozone absorption; thus, these models correct for the small additive scattering component in TM4 without considering the larger losses due to absorption.

Statistical analyses using RMS error and Δ_m are useful for summarizing results, however, they tend to mask the trends present in the original data. Scattergrams of satellite- and aircraft-based reflectance factors highlight the bias of the correc-

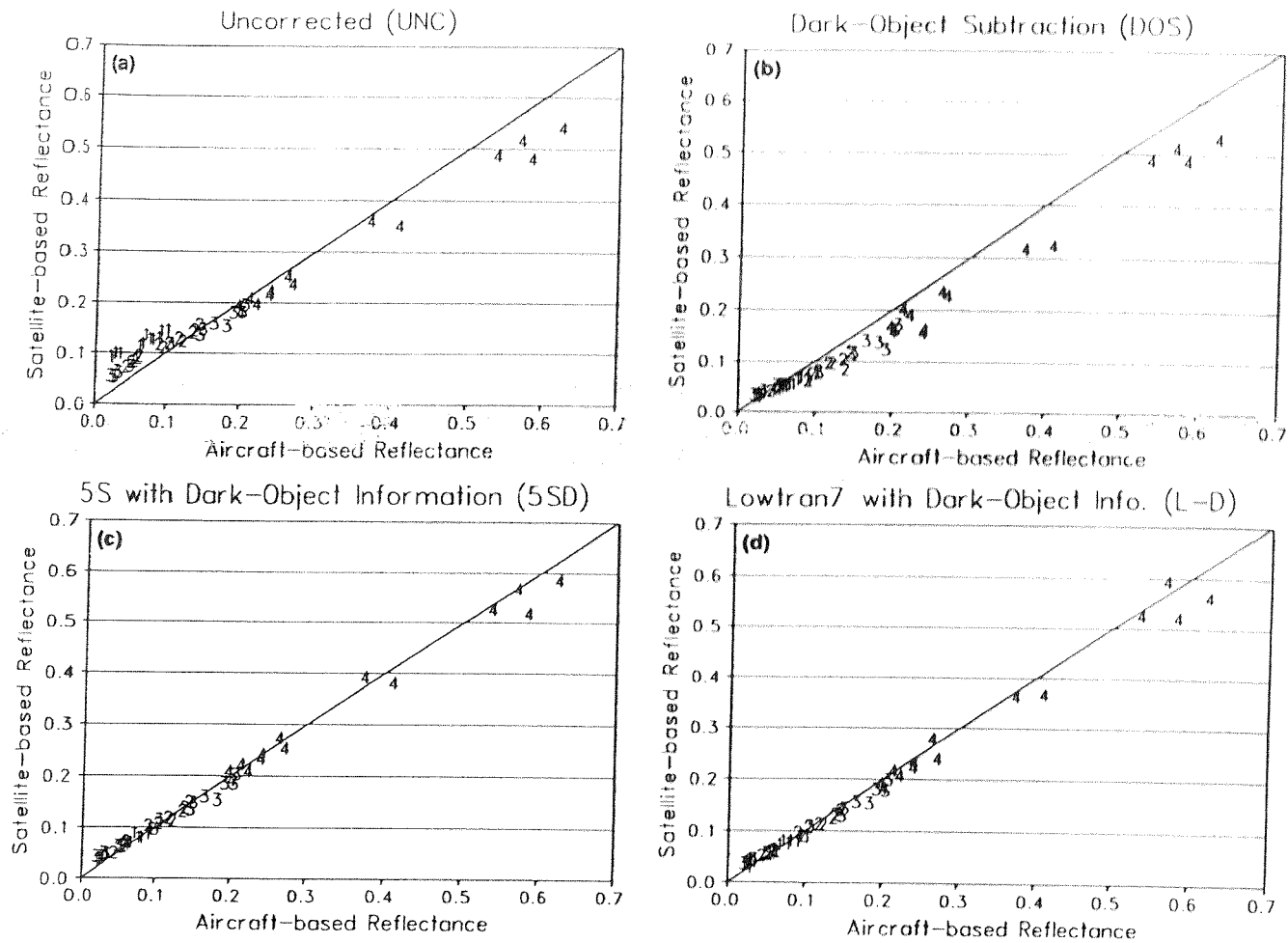


Figure 4. Satellite- and aircraft-based reflectance factor estimates for four bands (TM1-TM4), two targets (vegetated and bare soil), and seven dates. The solid line represents the one-to-one line and the numbers 1-4 correspond to TM spectral bands TM1-TM4.

tion procedures over the range of surface reflectance and spectral bands (Fig. 4). The most notable aspect of the reflectance data is the tendency for target reflectances to be low in TM1-TM3 bands and higher in TM4. This is a typical signature for most vegetated targets. The scattergrams also emphasize three aspects of atmospheric correction. First, for uncorrected satellite data, scattering increases apparent reflectance in TM1 and absorption decreases apparent reflectance in TM4. Second, a weakness of the DOS method is that it accounts only for path radiance effects, resulting in decreases in satellite-based reflectance over all bands. Third, the application of RTC-based corrections (such as L-D and 5SD) tended to bring the slope of the data closer to 1, the interceptor closer to 0, and decrease the overall scatter of the points.

Is Any Correction Better than None?

There have been suggestions that, for low reflectance scenes (roughly 0.0 to 0.1), a Rayleigh correction or any reasonable correction based on rough estimates of atmospheric conditions and a multiple-scattering radiative transfer code would improve estimates of surface reflectance from satellite-based data (Hovis, 1985; Slater, 1988). For the MAC data set (Table 4), the surface reflectance factors ranged from approximately 0.02 to 0.65 in TM1-TM4. When the analysis was limited to the reflectance range of 0.02 to 0.20 (Fig. 5), the RMS errors of nearly all the correction methods were reduced, resulting in RMS errors close to 0.01. Over the limited reflectance range, the DOS procedure resulted in lower error than uncorrected values, unlike the results over the entire reflectance range (Fig. 2c).

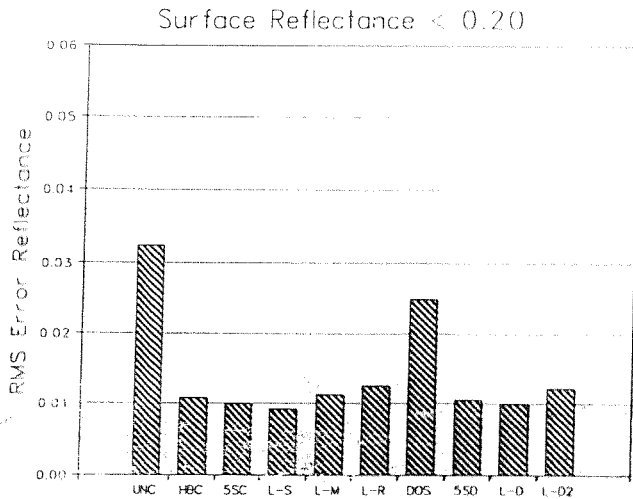


Figure 5. Root mean squared (RMS) error of reflectance factor estimation for data limited to surface reflectances < 0.20 , using all correction methods. RMS error was computed for 42 points, mostly within the visible spectrum. X-axis labels are defined in Table 6.

Unfortunately, by limiting the reflectance range to < 0.20 , nearly all the near-IR data (TM4) were eliminated. Thus, the general improvement in correction results may be attributed to 1) the larger Rayleigh contribution (relative to the aerosol contribution) and the accurately determined Rayleigh correction at short wavelengths and low reflectances and 2) the avoidance of water vapor absorption in this wavelength range. Referring to Figure 3, it is apparent that the Rayleigh-only correction (L-R) is most effective for TM1-TM3, due to the relative spectral contributions of Rayleigh and aerosol scattering in this wavelength range.

CONCLUDING REMARKS

Overall, these results emphasized the importance of using multiple-scattering radiative transfer codes for retrieval of surface reflectance and radiance from satellite-based sensors. They also stress the importance of selecting a correction method to suit the selected spectral bands and geographic location. For example, the dark-object subtraction technique is appropriate for correction of TM1, where attenuation is primarily due to scattering. For TM4, scattering is minimal, and absorption by water vapor is dominant; thus dark-object subtraction and simple Rayleigh corrections can produce greater error than no correction at all.

On the other hand, the three radiative transfer codes (RTCs) tested in this analysis were all successful in reducing the overall error of reflectance estimation. As expected, combining RTCs with on-site atmospheric optical depth measurements produced the most accurate estimates of surface reflectance, but RTCs with reasonable estimates of atmospheric conditions were surprisingly successful. When care was taken to choose appropriate models for water vapor and aerosol profiles, surface reflectance was evaluated to within ± 0.02 reflectance (1σ RMS).

An attempt was made to combine the image-based nature of the DOS technique with the accuracy of a radiative transfer code [based on work by Ahern et al. (1977)]. Using the histogram lower bound to provide information about atmospheric conditions, the Lowtran7 and 5S codes were used to compute surface reflectance from at-satellite radiance to within ± 0.015 . However, these methods showed some sensitivity to the assumption of dark-object surface reflectance, implying that knowledge of the dark-object reflectance is necessary for proper application of the methods.

Finally, it should be emphasized that these results were site-specific since they were achieved under relatively clear, dry conditions in central Arizona. Furthermore, though the MAC fields were relatively large ($0.27 \text{ km} \times 1.6 \text{ km}$) and highly uniform within field boundaries, the Maricopa area is characterized by finite fields of variable reflectance. This could lead to inherent errors in retrieval of surface reflectance factors from satellite-based digital data due to the combined effects of turbidity, background reflectance, and field size (Kaufman and Fraser, 1984).

We wish to acknowledge the excellent support and cooperation of the Maricopa Agricultural Center (MAC) personnel. We also acknowledge the field and laboratory assistance of Ron Seay, Tom Clarke, Stephanie Johnson, and Harold Kelly of the U.S. Water Conservation Laboratory and David Ammon, David Gellman, and Stuart Biggar of University of Arizona. Some of these data were initially processed by Ron Holm (Jet Propulsion Laboratory, Pasadena, California). We also thank two anonymous reviewers for their helpful comments and suggestions.

REFERENCES

- Ahern, F. J., Goodenough, D. G., Jain, S. C., Rao, V. R., and Rochon, G. (1977). Use of clear lakes as standard reflec-

- tors for atmospheric measurements, in *Proc. 11th Int. Symp. on Remote Sens. of Environ.*, Ann Arbor, MI, pp. 731-755.
- Biggar, S. F. (1990), In-flight methods for satellite sensor absolute radiometric calibration, Ph.D. dissertation, Univ. of Arizona, Tucson, 150 pp.
- Biggar, S. F., Gellman, D. I., and Slater, P. N. (1990), Improved evaluation of optical depth components from Langley plot data, *Remote Sens. Environ.* 32:91-101.
- Chandrasekhar, S. (1950), *Radiative Transfer*, Oxford Univ. Press, New York, 393 pp.
- Chavez, P. S., Jr. (1988), An improved dark-object subtraction technique for atmospheric scattering correction of multispectral data, *Remote Sens. Environ.* 24:459-479.
- Chavez, P. S., Jr. (1989), Radiometric calibration of Landsat Thematic Mapper multispectral images, *Photogramm. Eng. Remote Sens.* 55:1285-1294.
- Dozier, J., and Frew, J. (1981), Atmospheric corrections to satellite radiometric data over rugged terrain, *Remote Sens. Environ.* 11:191-205.
- Eltzman, L. (1968), UV, visible and IR attenuation for altitudes to 50 km, Report AFCRL-68-0153, Air Force Cambridge Research Laboratories, Bedford, MA, 49 pp.
- Herman, B. M., and Browning, S. R. (1965), A numerical solution to the equation of radiative transfer, *J. Atmos. Sci.* 22:59-66.
- Holm, R. G. (1987), The absolute radiometric calibration of space-based sensors, Ph.D. Dissertation, Univ. of Arizona, Tucson, 173 pp.
- Holm, R. G., Moran, M. S., Jackson, R. D., Slater, P. N., Yuan, B., and Biggar, S. F. (1989), Surface reflectance factor retrieval from Thematic Mapper data, *Remote Sens. Environ.* 27:47-57.
- Hovis, W. A. (1985), Landsat-4 Thematic Mapper calibration and atmospheric correction, in *Landsat-4 Science Characterization Early Results*, Vol. III, Pt. 2, pp. 411-420.
- Jackson, R. D. (1990), The MAC experiments, *Remote Sens. Environ.* 32:77-79.
- Jackson, R. D., Moran, M. S., Slater, P. N., and Biggar, S. F. (1987), Field calibration of reference reflectance panels, *Remote Sens. Environ.* 22:145-158.
- Jennings, S. G., Pinnick, R. G., and Auvermann, H. J. (1978), Effects of particulate complex refractive index and particle size distribution variations on atmospheric extinction and absorption for visible through middle IR wavelengths, *Appl. Opt.* 17:3922-3929.
- Kaufman, Y. J. (1985), The atmospheric effect on the separability of field classes measured from satellites, *Remote Sens. Environ.* 18:21-34.
- Kaufman, Y. J., and Fraser, R. S. (1984), Atmospheric effect on classification of finite fields, *Remote Sens. Environ.* 15: 95-118.
- Kneizys, F. X., Shettle, E. P., Abreu, L. W., et al. (1988), Users guide to LOWTRAN 7, Report AFGL-TR-88-0177, Air Force Cambridge Research Laboratories, Bedford, MA, August, 137 pp.
- Mateer, C. L., DeLuise, J. J., and Porco, C. C. (1980), The short Umkehr method, part I: Standard ozone profiles for use in the estimation of ozone profiles by the inversion of short Umkehr observations, NOAA Technical Memorandum, ERL ARL-86, July.
- Moran, M. S. (1986), The MAC experiment, *Remote Sens. Newsletter* (Univ. of Arizona, Tucson) 86:1-9.
- Moran, M. S., Jackson, R. D., Hart, G. F., et al. (1990), Obtaining surface reflectance factors from atmospheric and view angle corrected SPOT-1 HRV data, *Remote Sens. Environ.* 32:203-214.
- Ottensmider, J., and Fraser, R. S. (1976), Earth-atmosphere system and surface reflectivities in arid regions from LANDSAT MSS data, *Remote Sens. Environ.* 5:247-266.
- Palmer, J. M. (1984), Effective bandwidths for Landsat-4 and Landsat D' multispectral scanner and Thematic Mapper subsystem, *IEEE Trans. Geosci. Remote Sens.* GE-22:336-338.
- Pinter, P. J., Jr., Jackson, R. D., and Moran, M. S. (1990), Bidirectional reflectance factors of agricultural targets: a comparison of ground-, aircraft-, and satellite-based observations, *Remote Sens. Environ.* 32:215-228.
- Post, D. F., Mack, C., Camp, P. D., and Suliman, S. (1988), Mapping and characterization of the soils on the University of Arizona Maricopa Agricultural Center, in *Proc. Hydrol. and Water Res. in Arizona and the Southwest*, Arizona-Nevada Acad. of Sci., Vol. 18, pp. 48-60.
- Richardson, A. J. (1982), Relating Landsat digital count values to ground reflectance for optically thin atmospheric conditions, *Appl. Opt.* 21:1457-1462.
- Richter, R. (1990), A fast atmospheric correction algorithm applied to Landsat TM images, *Int. J. Remote Sens.* 11: 159-166.
- Singh, S. M. (1988), Estimation of multiple reflection and lowest order adjacency effects on remotely-sensed data, *Int. J. Remote Sens.* 9:1433-1450.
- Sissenwine, N., Grantham, D. D., and Salmela, H. A. (1968), *Humidity up to the mesopause*, Report AFCRL-68-0050, Air Force Surveys in Geophysics No. 206, Air Force Cambridge Research Laboratories, Bedford, MA.
- Slater, P. N. (1980), *Remote Sensing—Optics and Optical Systems*, Addison-Wesley, Reading, MA, 575 pp.
- Slater, P. N. (1988), Radiometric calibration requirements and atmospheric correction, *Proc. SPIE* 924:144-150.
- Slater, P. N., Biggar, S. F., Holm, R. G., et al. (1986), Absolute radiometric calibration of the Thematic Mapper, *Proc. SPIE* 660:2-8.
- Slater, P. N., Biggar, S. F., Holm, R. G., et al. (1987), Reflectance- and radiance-based methods for the in-flight absolute calibration of multispectral sensors, *Remote Sens. Environ.* 22:11-37.
- Tanré, D., Deroo, C., Dahuat, P., et al. (1985), Effets atmosphériques en télédétection-logiciel de simulation de

- signal satellitaire dans le spectre solaire, in *Proc. Third Intl. Colloq. on Spec. Signatures of Objects in Remote Sens.*, ESA SP-247, pp. 315-319.
- Teillet, P. M. (1986), Image correction for radiometric effects in remote sensing, *Int. J. Remote Sens.* 7:1637-1651.
- Teillet, P. M., and Santer, R. P. (1991), Terrain elevation and sensor altitude dependence in a semi-analytical atmospheric code, *Can. J. Remote Sens.* 17:36-44.
- Vincent, R. K. (1972), An ERTS Multispectral Scanner experiment for mapping iron compounds, in *Proc. of the 8th Int. Symp. on Remote Sens. of Environ.*, Ann Arbor, MI, pp. 1239-1247.